

# Simulation of astrophysical jet using the special relativistic hydrodynamics code

Orhan Donmez, Refik Kayali

*Nigde University Faculty of Art and Science, Physics Department, Nigde, Turkey*

(Dated: October 12, 2018)

This paper describes a multidimensional hydrodynamic code which can be used for the studies of relativistic astrophysical flows. The code solves the special relativistic hydrodynamic equations as a hyperbolic system of conservation laws based on High Resolution Shock Capturing (HRSC) Scheme. Two standard tests, one of which is the relativistic blast wave tested in our previous paper[1], and the other is the collision of two ultrarelativistic blast waves tested in here, are presented to demonstrate that the code captures correctly and gives solution in the discontinuities, accurately.

The relativistic astrophysical jet is modeled for the ultrarelativistic flow case. The dynamics of jet flowing is then determined by the ambient parameters such as densities, and velocities of the jets and the momentum impulse applied to the computational surface. We obtain solutions for the jet structure, propagation of jet during the time evolution, and variation in the Mach number on the computational domain at a fixed time.

## I. INTRODUCTION

Many high-energy astrophysical problems(SNRs,  $\gamma$ -ray bursts -GRBs, Active Galactic Nuclei (AGN) hot spots, etc.) involve relativistic flows, and thus understanding relativistic flows is important for interpreting the astrophysical phenomena correctly. For instance, intrinsic beam velocities typically larger than  $0.9c$  are required to explain the apparent superluminal motions observed in relativistic jets in microquasars in Galaxies[2] as well as in extragalactic radio sources associated with AGN. The shocks created during these phenomena accelerate particles which emit the observed radiation. In particular, it is widely accepted that the recently discovered GRBs afterglow results from an emission by relativistic shocks, created by the interaction between an initial ejecta and the interstellar medium.

The recent observations of GRB afterglow have lead to numerous attempts to model these phenomena.

General relativistic effects must be considered when strong gravitational fields are encountered as, for example, in the case of coalescing neutron stars or near black holes. The significant gravitational wave signal produced by some of these phenomena can also only be understood in the framework of the theory of general relativity. Another field of research, where special relativistic flows are encountered, is heavy-ion collision experiments performed with large particle accelerators. The heavy-ions are accelerated up to ultra-relativistic velocities to study various aspects of heavy-ion collision physics (e.g., multi-particle production, the occurrence of nuclear shock waves, collective flow phenomena, or dissipative processes) to explore the equation of state for hot dense nuclear matter, and to find evidence for the existence of the quark-gluon plasma.

Multi-wavelength observation of extragalactic jets performed in radio, optical and X-ray bands have extended dramatically our knowledge about the complex phenomenology of these objects. By means of these observations, different kinds of objects that can house these jets have been characterized, at the moment we can classify distinctly these sources as radio galaxies and quasars. A deeper analysis of these and other related objects led us to the idea of AGN. The images obtained from Hubble Space Telescope revealed a new detail in gas flow and shock wave patterns involving astrophysical jets and colliding interstellar winds of particles. Astrophysical jets are defined as highly collimated outflows in the form of high velocity mass flows. The outflows are observed in young stellar objects, proto-planetary nebula, compact objects, AGN, and GRBs[3] [5]. The jets include high Mach number and interact with surrounding ambient gas[6].

Simulating the fluid flow and shock wave patterns and detailed temperature profiles by implementing theoretical models in a gas dynamics simulator will help in analyzing the processes at work in these astrophysical objects. In these investigations, we apply the HRSC scheme with appropriate initial and boundary conditions to simulate relativistic astrophysical jets with high Mach number from the compact objects. Pioneered in this field Ref.[4] is the pioneer in this field. They were able to show that a flow of supersonic plasma remains stable and develops features that could be identified with the features in the observations of radio galaxies. A circular and canonical deceleration area called Mach disk as the hot spot, which is a strongly collimated beam as the elongated structure of the jets,

and a big zone of exhaust material as the lobes of radio galaxies[7]. Meanwhile, more physics has been included in the calculations such as the parameters varying in the perpendicular to the jet flow direction, the jet radius magnetic field [8][9] and the special relativistic effects[10][11]. Jets inside massive star, observed and called highly relativistic jets, have been studied numerically in both Newtonian[12] [13] and relativistic[14] [15] simulations and it has been shown that the collapsed model is able to explain many of the observed characteristic of GRBs. The collapsar is formed when the iron core of a rotating massive star collapses to black hole and an accretion disk. The explosive deaths of massive stars produce relativistic jets. These studies are also declared that the interaction of jet with the matter at the stellar surface and the stellar wind could carry the information for activities. The cocoon of the jet would also have different properties and the shocks within cocoon and jet could lead to  $\gamma$ -ray and  $x$ -ray transients.

In this paper, our goal is to simulate the ultrarelativistic jet problem using the already existing code which solves fully special relativistic hydrodynamics equations with HRSC scheme.

## II. FORMULATION

A general technical description of the Hydrodynamic equation is given by Donmez[1] as they will be used in our code development and the analytic description of different problems. The GRH equations are written in the standard covariant form, consist of the local conservation laws of the stress-energy tensor  $T^{\mu\nu}$  and the matter current density  $J^\mu$ :

$$\nabla_\mu T^{\mu\nu} = 0, \quad \nabla_\mu J^\mu = 0. \quad (1)$$

Greek indices run from 0 to 3, Latin indices from 1 to 3, and units in which the speed of light  $c = 1$  are used.  $\nabla_\mu$  stands for the covariant derivative with respect to the 4-metric of the underlying spacetime,  $g_{\mu\nu}$ .

Defining the characteristic waves of the general relativistic hydrodynamical equations is not trivial with imperfect fluid stress-energy tensor. The viscosity and heat conduction effects are neglected. This defines the perfect fluid stress-energy tensor. This stress-energy tensor is used to derive the hydrodynamical equations. Using perfect fluid stress-energy

tensor, we can solve some problems which are solved by the Newtonian hydrodynamics with viscosity, such as those involving angular momentum transport and shock waves on an accretion disk, etc. Entropy for perfect fluid is conserved along the fluid lines. The stress energy tensor for a perfect fluid is given as

$$T^{\mu\nu} = \rho h u^\mu u^\nu + P g^{\mu\nu}. \quad (2)$$

A perfect fluid is a fluid that moves through spacetime with a 4-velocity  $u^\mu$  which may vary from event to event. It exhibits a density of mass  $\rho$  and isotropic pressure  $P$  in the rest frame of each fluid element.  $h$  is the specific enthalpy, defined as

$$h = 1 + \epsilon + \frac{P}{\rho}. \quad (3)$$

Here  $\epsilon$  is the specific internal energy. The equation of state might have the functional form  $P = P(\rho, \epsilon)$ . The perfect gas equation of state,

$$P = (\Gamma - 1)\rho\epsilon, \quad (4)$$

is such a functional form.

The conservation laws in the form given in Eq.(1) are not suitable for the use in advanced numerical schemes in  $2D$ . In order to carry out numerical hydrodynamic evolutions and to use HRSC methods, the hydrodynamic equations after the 2+1 split must be written as a hyperbolic system of first order flux conservative equations. The Eq.(1) is written in terms of coordinate derivatives, using the coordinates  $(x^0 = t, x^i)$  where and rest of the paper  $i = 1, 2$  and  $j = 1, 2$ . Eq.(1) is projected onto the basis  $\{n^\mu, (\frac{\partial}{\partial x^i})^\mu\}$ , where  $n^\mu$  is a unit timelike vector normal to a given hypersurface. After a straightforward calculation conservation form of Special Relativistic Hydrodynamical (SRH) equation can be written,

$$\partial_t \vec{U} + \partial_x \vec{F}^x + \partial_y \vec{F}^y = 0, \quad (5)$$

where  $\partial_t = \partial/\partial t$  and  $\partial_x = \partial/\partial x^x$ . This basic step serves to identify the set of unknowns, the vector of conserved quantities  $\vec{U}$ , and their corresponding fluxes  $\vec{F}(\vec{U})$ . With the equations in conservation form, almost every high resolution method devised to solve hyperbolic systems of conservation laws can be extended to SRH.

The evolved state vector  $\vec{U}$  consists of the conservative variables  $(D, S_x, S_y, \tau)$  which are conserved variables for density, momentum in  $x$  and  $y$  direction and energy respectively; in terms of the primitive variables  $(\rho, v^x, v^y, \epsilon)$ , this becomes,

$$D = \sqrt{\gamma}W\rho; \quad S_x = \sqrt{\gamma}\rho hW^2v_x; \quad S_y = \sqrt{\gamma}\rho hW^2v_y; \quad \tau = \sqrt{\gamma}(\rho hW^2 - P - W\rho) \quad (6)$$

Here  $\gamma$  is the determinant of the 3-metric  $\gamma_{ij}$ , which is unitary matrix,  $v_x$  and  $v_y$  are the fluid 3-velocity, the lapse function  $\alpha = 1$  and the shift vector  $\beta = 0$  for SRH and  $W$  is the Lorentz factor,

$$W = \alpha u^0 = (1 - v^i v^j)^{-1/2}. \quad (7)$$

The flux vectors  $\vec{F}^i$  are given by

$$\vec{F}^i = \begin{pmatrix} v^i D \\ v^i S_j + P \delta_j^i \\ (v^i \tau + v^i P) \end{pmatrix}. \quad (8)$$

The spatial components of the 4-velocity  $u^i$  are related to the 3-velocity by the following formula:  $u^i = W v^i$ . The source vector  $\vec{S} = 0$  for SRH case.

### A. Spectral Decomposition and Characteristic Fields

The use of HRSC schemes requires the spectral decomposition of the Jacobian matrix of the system,  $\partial \vec{F}^i / \partial \vec{U}$ . The spectral decomposition of the Jacobian matrices of the SRH equations with a general equation of state was reported here . It is displayed the spectral decomposition, valid for a generic spatial metric, in the  $x$ -direction,  $(\partial \vec{F}^x / \partial \vec{U})$ ; permutation of the indices yields the  $y$  direction.

We started the solution by considering an equation of state in which the pressure  $P$  is a function of  $\rho$  and  $\epsilon$ ,  $P = P(\rho, \epsilon)$ . The relativistic speed of sound in the fluid  $C_s$  is given by

$$C_s^2 = \left. \frac{\partial P}{\partial E} \right|_S = \frac{\chi}{h} + \frac{P\kappa}{\rho^2 h}, \quad (9)$$

where  $\chi = \partial P / \partial \rho|_\epsilon$ ,  $\kappa = \partial P / \partial \epsilon|_\rho$ ,  $S$  is the entropy per particle, and  $E = \rho + \rho\epsilon$  is the total rest energy density.

A complete set of the right eigenvectors  $[\vec{r}_i]$  and corresponding eigenvalues  $\lambda_i$  along the  $x$ -direction obeys

$$\left[ \frac{\partial \vec{F}^x}{\partial \vec{U}} \right] [\vec{r}_i] = \lambda_i [\vec{r}_i], \quad i = 1, \dots, 4. \quad (10)$$

The solution contains triply degenerate eigenvalues,

$$\lambda_1^x = \lambda_2^x = \lambda_3^x = v^x. \quad (11)$$

The other eigenvalues are given as

$$\lambda_{\pm}^x = \frac{1}{1 - v^2 C_s^2} \left\{ v^x (1 - C_s^2) \pm \sqrt{C_s^2 (1 - v^2) [(1 - v^2 C_s^2) - v^x v^x (1 - C_s^2)]} \right\}. \quad (12)$$

A set of linearly independent right eigenvectors spanning this space is given as

$$\vec{r}_1^x = \left[ \frac{\kappa}{hW(\kappa - \rho C_s^2)}, v_x, v_y, 1 - \frac{\kappa}{hW(\kappa - \rho C_s^2)} \right]^T, \quad (13)$$

$$\vec{r}_2^x = \left[ Wv_y, h2W^2 v_x v_y, h(1 + 2W^2 v_y v_y), v_y W(2Wh - 1) \right]^T, \quad (14)$$

and

$$\vec{r}_{\pm}^x = \left[ 1, hW(v_x - \frac{v^x - \lambda_{\pm}}{1 - v^x \lambda_{\pm}}), hWv_y, \frac{hW(1 - v^x v^x)}{1 - v^x \lambda_{\pm}} - 1 \right]^T. \quad (15)$$

Here, the superscript T denotes the transpose.

Now, the eigenvalues and eigenvectors are computed in the  $y$ -direction using the information in the  $x$ -direction in Donmez [1] for general relativistic hydrodynamic equations. Let  $\mathbf{M}^1(U)$  be the matrix of the right eigenvectors, that is, the matrix having as columns the right eigenvectors with the standard ordering([1], [16]),  $\mathbf{M}^1 = (\vec{r}_-, \vec{r}_1, \vec{r}_2, \vec{r}_+)$ . To obtain the spectral decomposition in the other spatial directions  $q = 2(\equiv y)$ , it is enough to take into account the following symmetry relations:

- 1) The eigenvalues are easily obtained by carrying out in equations (11) and (12) a simple substitution of indices  $x$  by  $q$ .
- 2) The matrix  $M^1$  in the  $x$ -direction is permuted according to  $\mathbf{M}^q = \mathcal{P}_{q1}(\mathbf{M}^1)$ , where the two operators  $\mathcal{P}_{q1}$  act on their arguments by the following sequential operations:
  - to permute the second and  $(q + 1)$ th rows,
  - to interchange indices  $1 \equiv x$  with  $q$ .

From Donat et. al.[17], the left eigenvectors in the  $x$ -direction are :

$$\mathbf{l}_{0,1} = \frac{W}{\mathcal{K} - 1} \begin{bmatrix} h - W \\ Wv^x \\ Wv^y \\ -W \end{bmatrix} \quad (16)$$

$$\mathbf{l}_{0,2} = \frac{1}{h\xi^x} \begin{bmatrix} -v_y \\ v^x v_y \\ (1 - v_x v^x) \\ -v_y \end{bmatrix} \quad (17)$$

$$\mathbf{l}_{\mp} = (\pm 1) \frac{h^2}{\Delta^x} \begin{bmatrix} hW\mathcal{V}_{\pm}^x \xi^x + (\pm \frac{\Delta}{h^2}) l_{\mp}^{(5)} \\ \Gamma_{xx}(1 - \mathcal{K}\tilde{\mathcal{A}}_{\pm}^x) + (2\mathcal{K} - 1)\mathcal{V}_{\pm}^x(W^2 v^x \xi^x - \Gamma_{xx} v^x) \\ \Gamma_{xy}(1 - \mathcal{K}\tilde{\mathcal{A}}_{\pm}^x) + (2\mathcal{K} - 1)\mathcal{V}_{\pm}^x(W^2 v^y \xi^x - \Gamma_{xy} v^x) \\ (1 - \mathcal{K})[-\gamma v^x + \mathcal{V}_{\pm}^x(W^2 \xi^x - \Gamma_{xx})] - \mathcal{K}W^2 \mathcal{V}_{\pm}^x \xi^x \end{bmatrix} \quad (18)$$

The variables used for the left eigenvectors in the  $x$ -direction are defined as follows:

$$\mathcal{K} \equiv \frac{\tilde{\kappa}}{\tilde{\kappa} - c_s^2} \quad , \quad \tilde{\kappa} \equiv \kappa / \rho$$

$$\mathcal{C}_{\pm}^x \equiv v_x - \mathcal{V}_{\pm}^x \quad , \quad \mathcal{V}_{\pm}^x \equiv \frac{v^x - \lambda_{\pm}^x}{\gamma^{xx} - v^x \lambda_{\pm}^x}$$

$$\tilde{\mathcal{A}}_{\pm}^x \equiv \frac{1 - v^x v^x}{1 - v^x \lambda_{\pm}^x}$$

$$1 - \tilde{\mathcal{A}}_{\pm}^x = v^x \mathcal{V}_{\pm}^x \quad , \quad \tilde{\mathcal{A}}_{\pm}^x - \tilde{\mathcal{A}}_{\mp}^x = v^x (\mathcal{C}_{\pm}^x - \mathcal{C}_{\mp}^x)$$

$$(\mathcal{C}_{\pm}^x - \mathcal{C}_{\pm}^x) + (\tilde{\mathcal{A}}_{\mp}^x \mathcal{V}_{\pm}^x - \tilde{\mathcal{A}}_{\pm}^x \mathcal{V}_{\mp}^x) = 0$$

$$\Delta^x \equiv h^3 W (\mathcal{K} - 1) (\mathcal{C}_{+}^x - \mathcal{C}_{-}^x) \xi^x$$

$$\xi^x \equiv 1 - v^x v^x$$

Detailed informations related with numerical solution of GRH equations using high resolution shock capturing schemes in  $3D$  are given in our paper Donmez[1]. This reference



explains detail description of numerical solutions of SRH equations, Adaptive-Mesh Refinement, high resolution shock capturing method used, and solution of GRH equation using Schwarzschild coordinate as a source term. The code is constructed for general spacetime metric with lapse function and shift vector and is fully parallelized to make optimum use of supercomputers which is necessary to achieve the numerical modeling of real astrophysical problems, such as astrophysical jet problems, coalescing of the compact binaries and accretion disk around the compact objects.

### III. NUMERICAL RESULTS

#### A. Boundary Condition

Boundary conditions are set by filling the data in guard cells with appropriate values. In the numerical calculation, boundary filling plays an important role in the simulations. The computational grid is extended at both sides of the physical domain to compute the fluxes at interfaces. These extra cells are also called guard cells or ghost zones. In this paper, we have used outflow boundary condition at each ghost zone. This boundary condition has to be provided on each time step for all primitive and conservative variables in the special relativistic hydro code. The outflow boundary condition for the computational domain is as follows. For velocity:  $U_0^n = -\frac{1}{2}(|U_1^n| - U_1^n)$  and  $U_{M+1}^n = \frac{1}{2}(|U_M^n| + U_M^n)$ . For the other variables:  $U_0^n = U_1^n$  and  $U_{M+1}^n = U_M^n$ , where  $n$  represents the time step.

#### B. Relativistic Blast Wave

Riemann problems with large initial pressure jumps produce blast waves with dense shells of material propagating at relativistic speeds. The Riemann shock tube is a useful test problem because it has an exact time-dependent solution, and tests the ability of the code to evolve both smooth and discontinuous flows. For appropriate initial conditions, both the speed of the leading shock front and the velocity of the shell material approach the speed of light producing very narrow structures. The accurate description of these thin, relativistic shells involving large density contrasts is a challenge for any numerical code. Some particular blast wave problems have become standard numerical tests. One of the

common test problem is called the special relativistic shock tube problem. Testing the code with this problem is given our paper Donmez[1].

### C. Collision of two relativistic blast waves in 2D

The collision of two strong blast waves in one-dimension was used by Woodward et al.[18] to compare the performance of several numerical methods in classical hydrodynamics. In the relativistic case, Yang et al.[19] considered the same problem to test the high-order extensions of the relativistic beam scheme, whereas Marti et al.[20] used it to evaluate the performance of their relativistic PPM code. In the last treatment, the original boundary conditions were changed (from reflecting to outflow) to avoid the reflection and subsequent interaction of rarefaction waves allowing for a comparison with an analytical solution. The initial data corresponding to this test, consisting of three constant states with large pressure jumps at the discontinuities separates the states.

In this report, the initial data corresponds to collision of two strong blast waves in 2D, consisting of three constant states with large pressure jumps at the discontinuities separating the states (at  $r = 0.15$  and  $r = 0.85$ , where  $r = \sqrt{y^2 + z^2}$ ), as well as containing the properties of the blast waves created by the decay of the initial discontinuities which are located on the main diagonal of the square box and the data is extracted along the other diagonal axis. The initial data for this test is listed in Table I. The initial pressure discontinuities drive shocks into the middle part of the grid; behind them, rarefaction form and propagate toward the outer boundaries where they are falling out from computational domain. When the two shock waves collided at  $t = 0.41$ , a very dense shell is created. The collision gives rise to a narrow region of very high density as seen in Fig.1 bounded by two shocks moving at speeds 0.88 (shock at the left) and 0.711 (shock at the right). The velocity of shock wave during the time evolution is plotted in the right panel of Fig.3. The presence of very narrow structures involving large density jumps requires very fine zoning and high resolution scheme to resolve the states properly. The high resolution shock capturing scheme we used here resolves the structure of the collision region satisfactorily well. Fig.2 shows that more resolutions are needed to resolve the preshock and postshock states reasonably well. The left panel at Fig.3 shows the behavior of pressure jump during the time evolution. The outflowing shock does not propagate along the grid and the contact discontinuity is not

created on the numerical results.

#### D. Astrophysical Jet

Investigation of gas flow in close binary systems is important in considering the accretion disk around the compact objects. The interaction of the disk with the compact objects, through processes that are still poorly understood, produces jets with high energy to mass ratio. Here we are primarily concerned with the propagation of these jets, not so much with how they are born. The propagating jets produce solar wind in the medium and this wind is highly supersonic. So obstacles in the flow, large variations in stream speeds, or fast ejecta produce shock waves, just as shock waves are produced by a supersonic jet. With a jet, sound waves develop ahead of the jet nose because the matter is traveling faster than the waves can escape. A shock wave forms, due to pressure buildup, to keep the air flowing around the jet.

Jets are, by current theory, the best, perhaps, essential method of explaining how such large amounts of energy can be observed from objects at cosmological distances. However, there is much speculation as to the exact nature of these jets, the primary questions being: how do they arise and what is their structure. In this paper, we focus on the question, what is the structure of GRB jets?

Here, we numerically model the  $2D$  simulation of a relativistic jet propagating through an homogeneous atmosphere. The initial computational domain and values of beam for the flow velocity, Mach number, rest-mass density and adiabatic index are given in Fig.4. The fluid viscosity and thermal conductivity are neglected. The ambient medium is has a size of  $10 \times 120$ . The jet is injected at  $4.8 < y < 5.2$  in the direction of positive  $z$ -axis. We have constructed a slab jet, which is periodic in the  $x$ - direction. An ideal gas equation of state with adiabatic index  $\gamma = 5/3$  is assumed to describe both the jet matter and the ambient gas. In our calculation, 256 resolution in  $y$  and 4096 resolution in  $z$  are used for Figs.5,9. It is well known that the propagation of a supersonic jet is governed by the interaction of jet matter with ambient medium, which produces a bow shock in the ambient medium. The evolution of the jet was simulated up to the time when the head of the jet is about to reach to the boundary, which is far away from the injection point.

The time evolution of relativistic jet for rest-mass density in the plane  $x = 0$  is given in

Fig.5 at different snapshots when the jet propagates through  $y - z$  plane. The presence of emitting matter moving at different velocities and orientations could lead to local variations of apparent relativistic motion within the jet. The distribution of apparent motions during the time evolutions is inhomogeneous and fringed as seen in Fig.5. The structure of jet contains cocoon and vortexes with a bow shock. The cocoon contains shocked jet material deflected backward at the head of the jet. Since the jet is narrowly collimated, its beam is very thin.

The Fig.6 shows the variations in one-dimensional cut of rest mass density in the jet propagation direction,  $z$ , at final snapshot for two different jet velocities,  $v = 0.5$  and  $v = 0.9$ . While the one with smaller velocity is called as a mildly relativistic jet, the other one is called the ultra-relativistic jet. The ultra-relativistic one displays rich internal structure with oblique shocks effectively decelerating the flow in the beam from Mach number equal to 140 at the injection point down to a value of about 10 around the head as seen in Fig.7. The one-dimensional cut of the rest-mass density as given in Fig.6 shows that the jet density propagates and oscillates on the working surface and it produces time varying waves and shock waves which interact with ambient medium. The pressure is larger at the head of jet and it causes the jet to propagate through the ambient medium at a larger speeds in both direction. The graphs seen in Fig.8 show the variation of the  $y$  velocity of cocoon, propagating through computational domain, at a fixed  $y = 5$  along the  $z$ -axis for four different times. The head of jet has the largest  $y$  velocity which is represented with peaks as seen in Fig.8. Figs.5, 6 and 7 also depict that there is a Mach shock at the jet head, and material that has passed through the head is slowly forming a backflow along the jet, building up the a shear layer.

We have also examined the propagation of two-dimensional relativistic jet in case of the different initial velocities and adiabatic values,  $\Gamma$ . The rest mass density for different  $\Gamma$  values are plotted in Fig.9. In agreement with previous studies on astrophysical problem, the relativistic jet is also more tightly packed with the smaller  $\Gamma$ . The lower  $\Gamma$  means cooler jet with larger Mach number of the flow. The cooler jet presents also a complex structure of internal shocks generated by pressure mismatches between the beam and the overpressured cocoon and by perturbations of the beam boundary by vortices and bulk motions within the cocoon. The cocoon is mainly formed by large vortices in cold jets with  $\Gamma = 5/3$  while the strong beam collimation causes a large acceleration of the jet in cold jets with  $\Gamma = 4/3$ .

The beam gas is less efficiently redirected into the cocoon, and thinner cocoon with smaller vortices form with  $\Gamma = 4/3$  as seen in Fig.9.

#### IV. CONCLUSION

We have described the main features of stable  $2D$  special relativistic hydrodynamical code and discussed test problems in Ref.[1] and here involving strong shocks in two-dimension. The test problem solved here is called the collision of relativistic blast wave. The promising results from the test problem give us encouragement to simulate ultrarelativistic gas flows.

We have carried out simulations of fully relativistic astrophysical jet in  $2D$ . By detailed examination of a time series of ultrarelativistic flow, we have described the propagation of jet through the computational domain. The ultrarelativistic flow is thought to occur and to play a crucial role in the generation of GRBs. We have also computed the dynamic of jet in case of different adiabatic index used in equation of state. The jet with  $\Gamma = 4/3$  form thinner cocoon with smaller vortices and the matter collimation causes a large acceleration of the jet.

#### Acknowledgments

This project is supported by N.U. 2003/01. It has been performed using TUBITAK/ULAKBIM super computers/Beowulf cluster.

- 
- [1] Dönmez, O., *Astrophysics and Space Science* **293** (2004) 323-354.
  - [2] Mirabel, I. F., & Rodriguez, L. F., *ARA&A* **37** (1999) 409
  - [3] Frank, A., Lery, T., Gardiner, T., A., Jones, T., W., and Ryu, D., *ApJ* **540** (2000) 342
  - [4] Norman, M., L., Smarr, K-H., Winkler, A., and Smith, M., D., *A&A* **113** (1982) 136-154
  - [5] Norman, M., L., *Annals of the New York Academy of Sciences* **617** (1990) 217
  - [6] Stone, J., M., and Norman, M., L., *ApJ* **413** (1993) 210

- [7] Ferrari, A., ARAA **36** (1998) 539-598
- [8] Clarke, D., A., Norman, M., L., and Burns, J., O., ApJ **311** (1986) L63-L67
- [9] Lind, K., R., Payne, D., G., Meier, D., L., and Blandford, R., D., ApJ **344** (1989) 89-103
- [10] Komissarov, S., S., MNRAS **308** (1999) 1069-1076
- [11] Aloy, M., A., Ibanez, J., Ma., Marti, J., Ma., Gomez, J., L., and Muller, E., ApJ **523** (1999) L125-L128
- [12] Khokhlov, A., M., Hflich, P., A., Oran, E., S., Wheeler, J., C., Wang, L., and Chtchelkanova, A., Yu, ApJ **524** (1999) 107
- [13] MaFadyen1, A., I., Woosley, S., E., ApJ **524** (1999) 262
- [14] Aloy, M., A., Mjller, E., Ibanez, J., M., Marti, J., M., and MacFadyen, A., ApJ **531** (2000) L119
- [15] Zhang, W., Woosley, S., E., and MacFadyen, A., I., ApJ **586** (2003) 356
- [16] F. Banyuls, J. A. Font, J. M. Ibanez, J.M. Marti, and J. A. Miralles, Astrophys. J. **476** (1997) 221.
- [17] R. Donat, J. A. Font, J. M. Ibanez, and A. Marquina, J.Comput. Phys. **146** (1998) 58.
- [18] Woodward, P.R., and Colella, P., J. Comput. Phys. **54** (1984) 115-173.
- [19] Yang, J.Y., Chen, M.H., Tsai, I.-N., and Chang, J.W., J. Comput. Phys. **136** (1997) 19-40.
- [20] Marti, J.M, and Muller, E., J. Comput. Phys. **123** (1996) 1-14.

TABLE I: Initial data for the two relativistic blast wave collision test problem in  $2D$ . The decay of the initial discontinuities (at  $r = 0.15$  and  $r = 0.85$ ) produces two shock waves (velocities  $v_{shock}$ ) moving in opposite directions. The gas is assumed to be ideal with an adiabatic index  $\gamma = 5/3$ .

Blast wave collision test problem			
	Left	Middle	Right
$\rho$	1.0	1.0	1.0
$p$	100.0	0.01	10.0
$v_x$	0.0	0.0	0.0
$v_y$	0.0	0.0	0.0

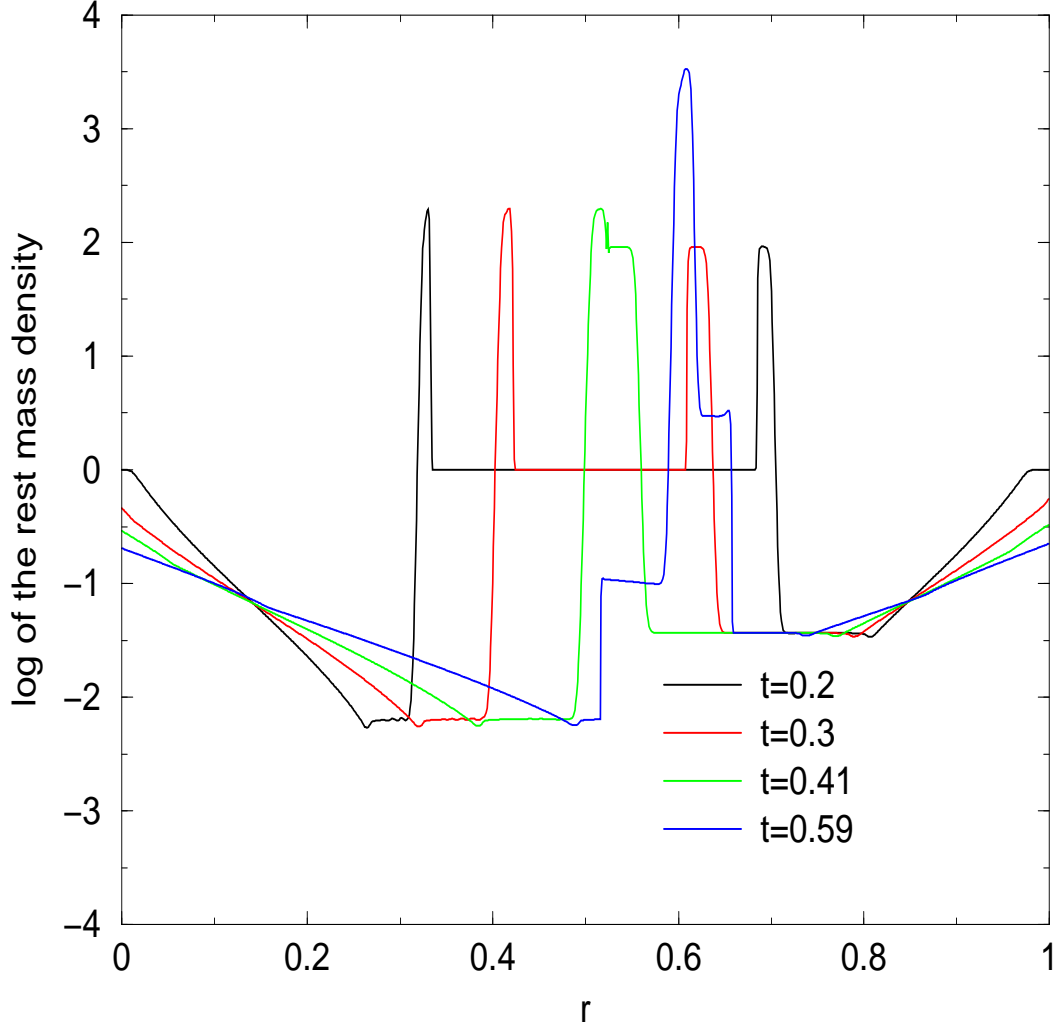


FIG. 1: The evolution of log of the density distribution for the colliding relativistic blast wave problem up to the interaction of the waves. The data is taken from the two-dimensional colliding wave extracting from the diagonal axis. The computation has been performed with relativistic hydrodynamical code on an equidistant grid of 1024 zones



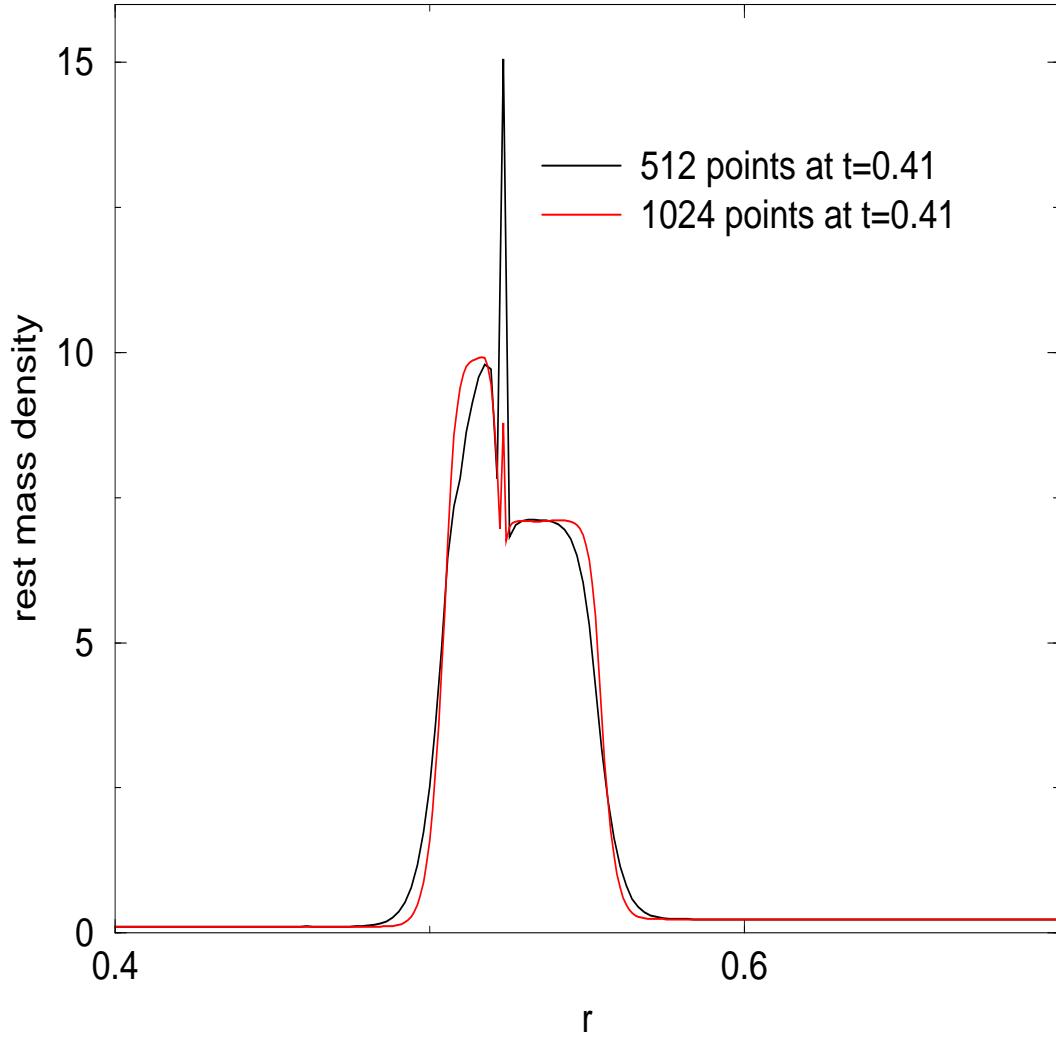


FIG. 2: The evolution of density at  $t = 0.41$  at different resolution. The preshock and postshock region are resolved with more grid zones.

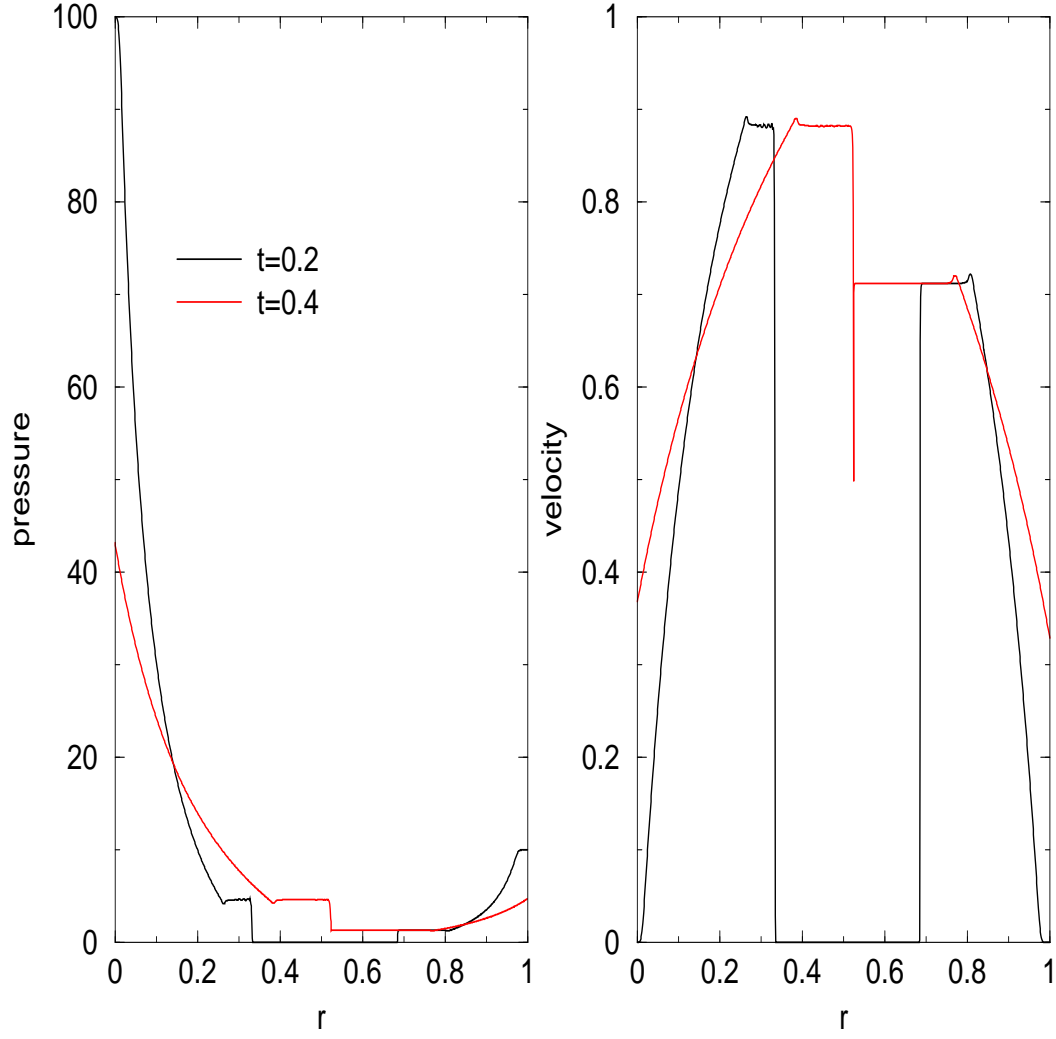


FIG. 3: The left pane: the evolution of pressure at two-different time. Right panel: the evolution of velocity of the blast wave.

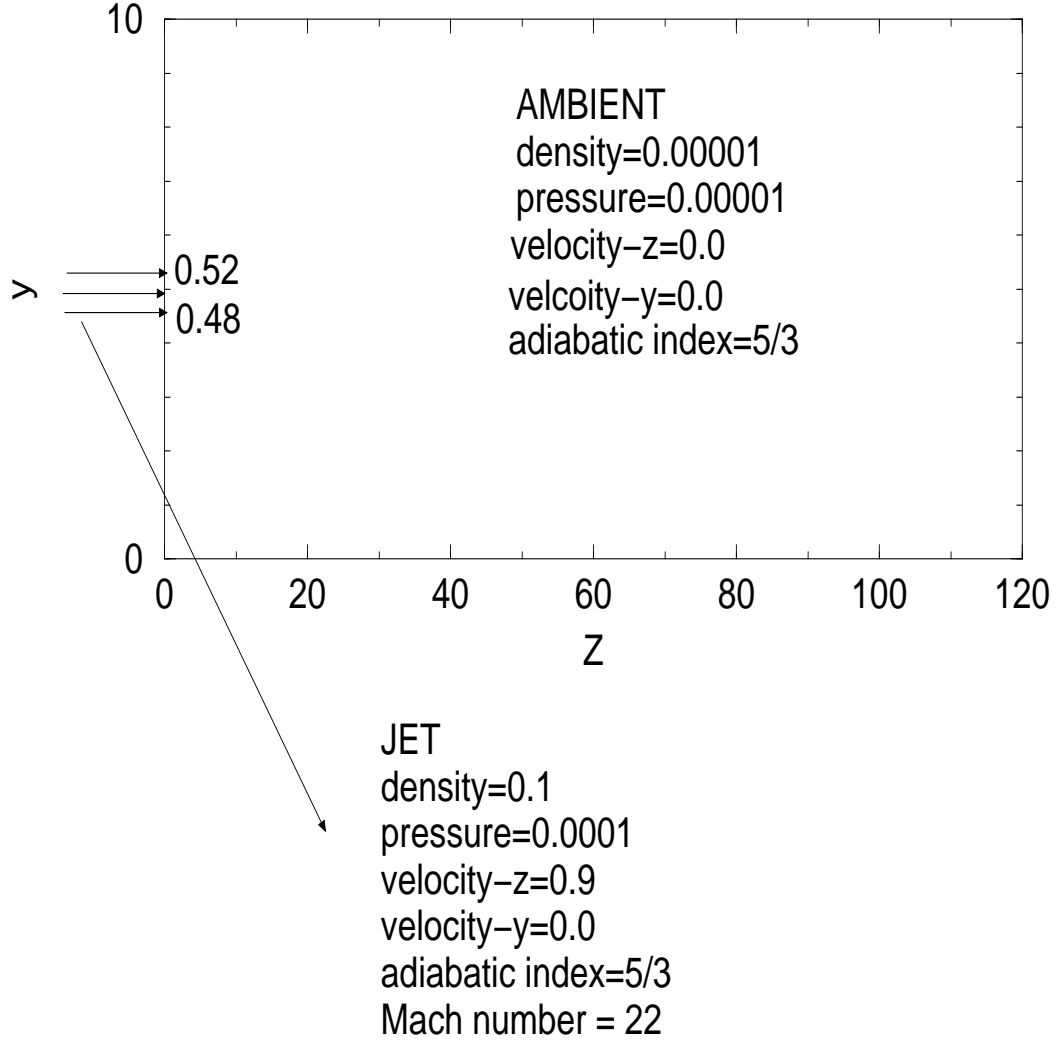


FIG. 4: Initial representation of computational domain for astrophysical jet with the appropriate initial conditions.

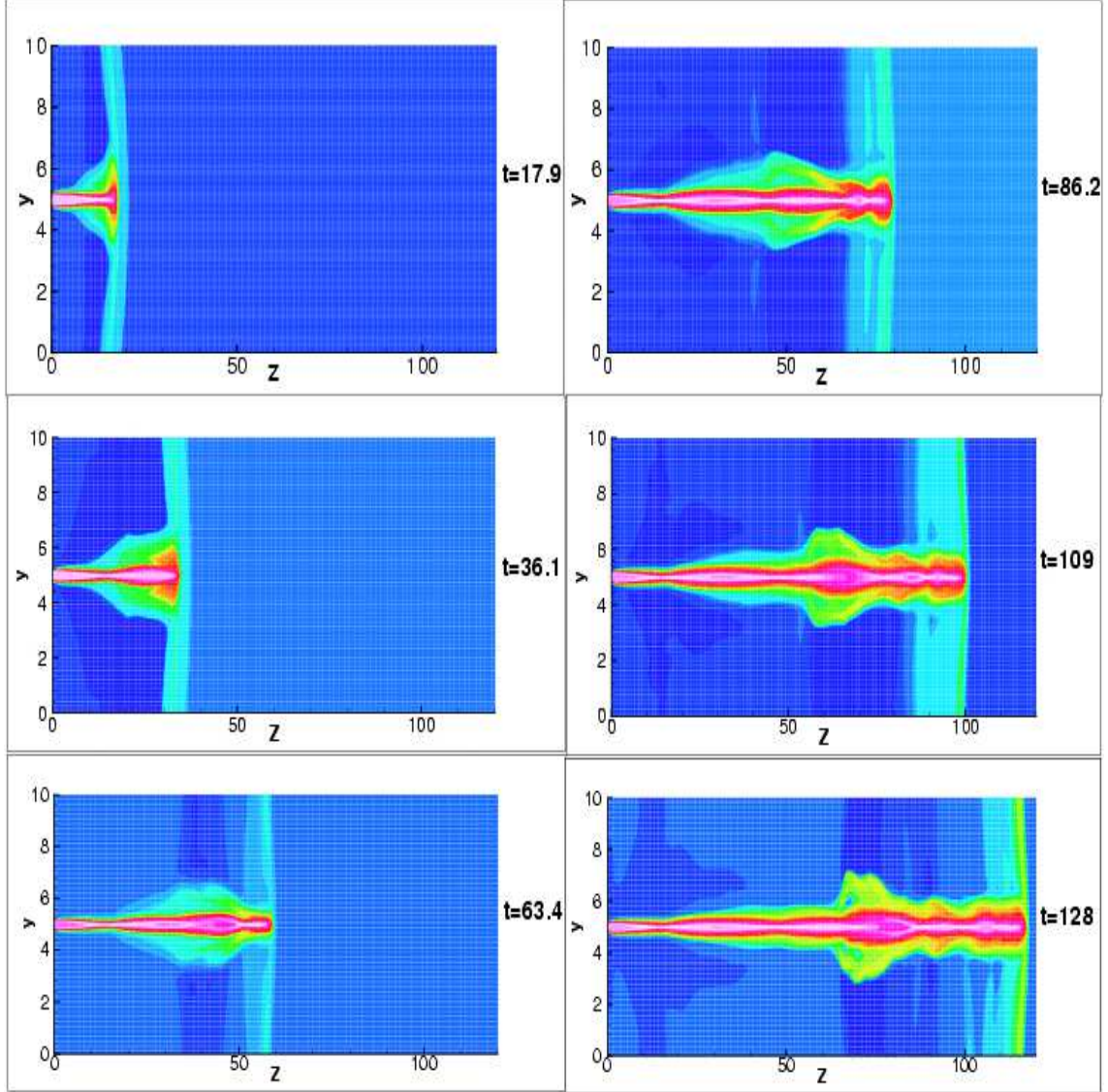


FIG. 5: Contour maps of the logarithm of the rest-mass density for relativistic jet, moving with  $v = 0.9c$ , at different times. Snapshots of the proper rest-mass density distribution are plotted at  $y - z$  plane. 256 resolutions in  $y$  and 4096 resolutions in  $z$  are used.

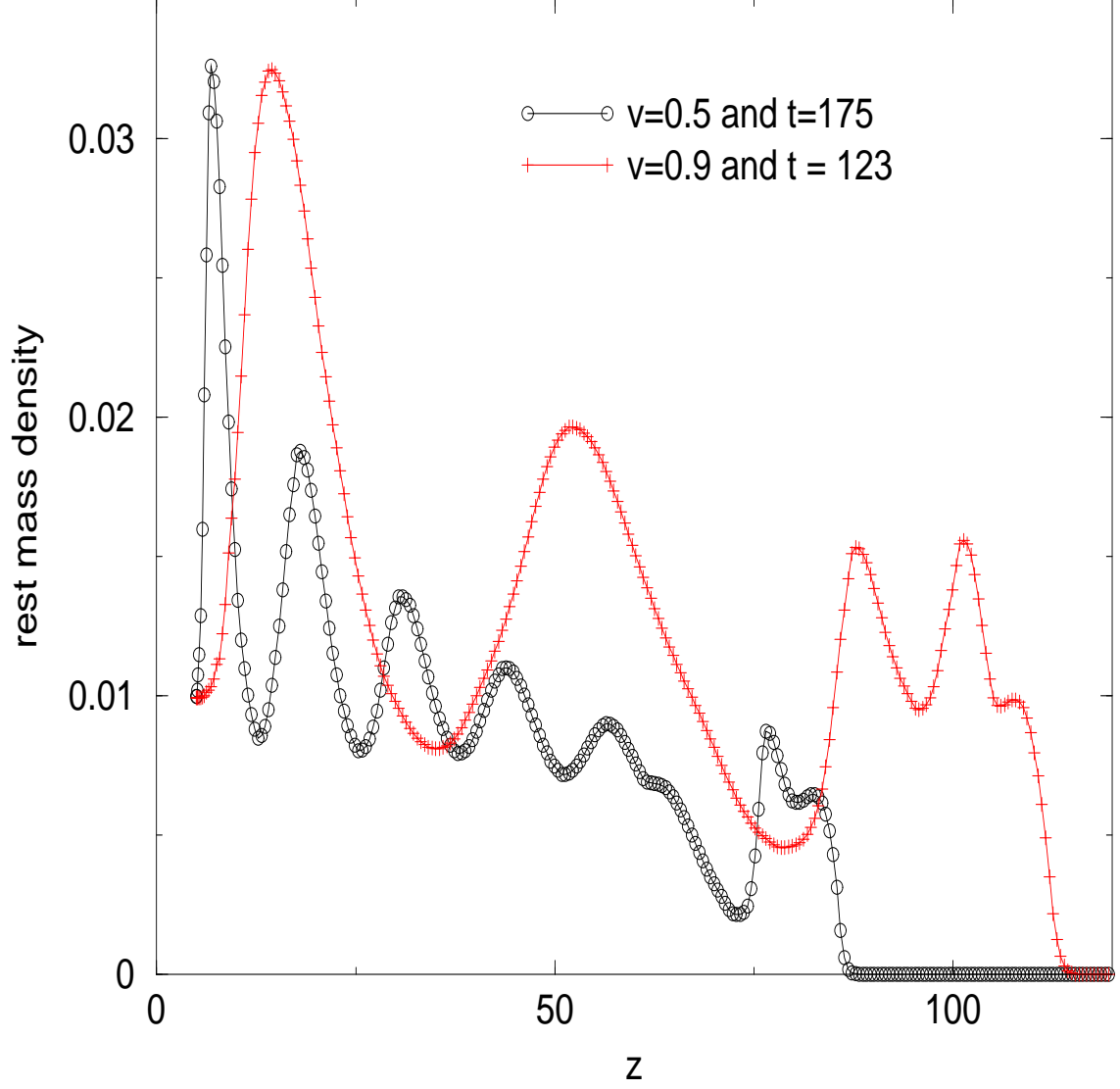


FIG. 6: Vertical configuration values of rest-mass density along a cut to the  $z$ -axis, at  $r = 5.0$ , are shown for different jet velocity (mildly and ultrarelativistic cases). This figure illustrates the value of rest mass density during the evolution of jet flow at fixed time. Oscillatory jet rest mass density is achieved.

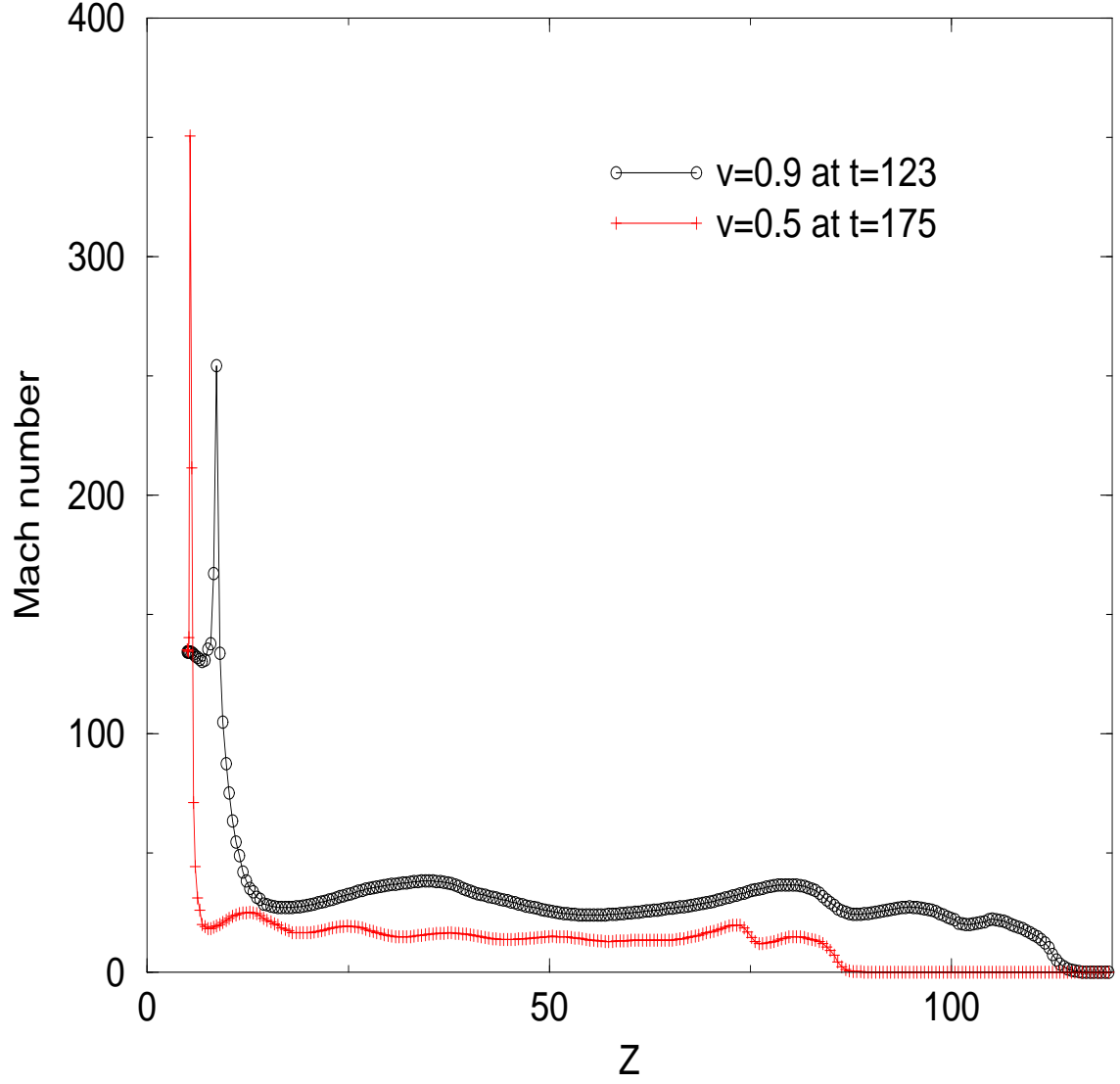


FIG. 7: Behavior of Mach number as a function of  $Z$  for different initial jet velocities at different times. It is taken at a fixed  $y=5.0$

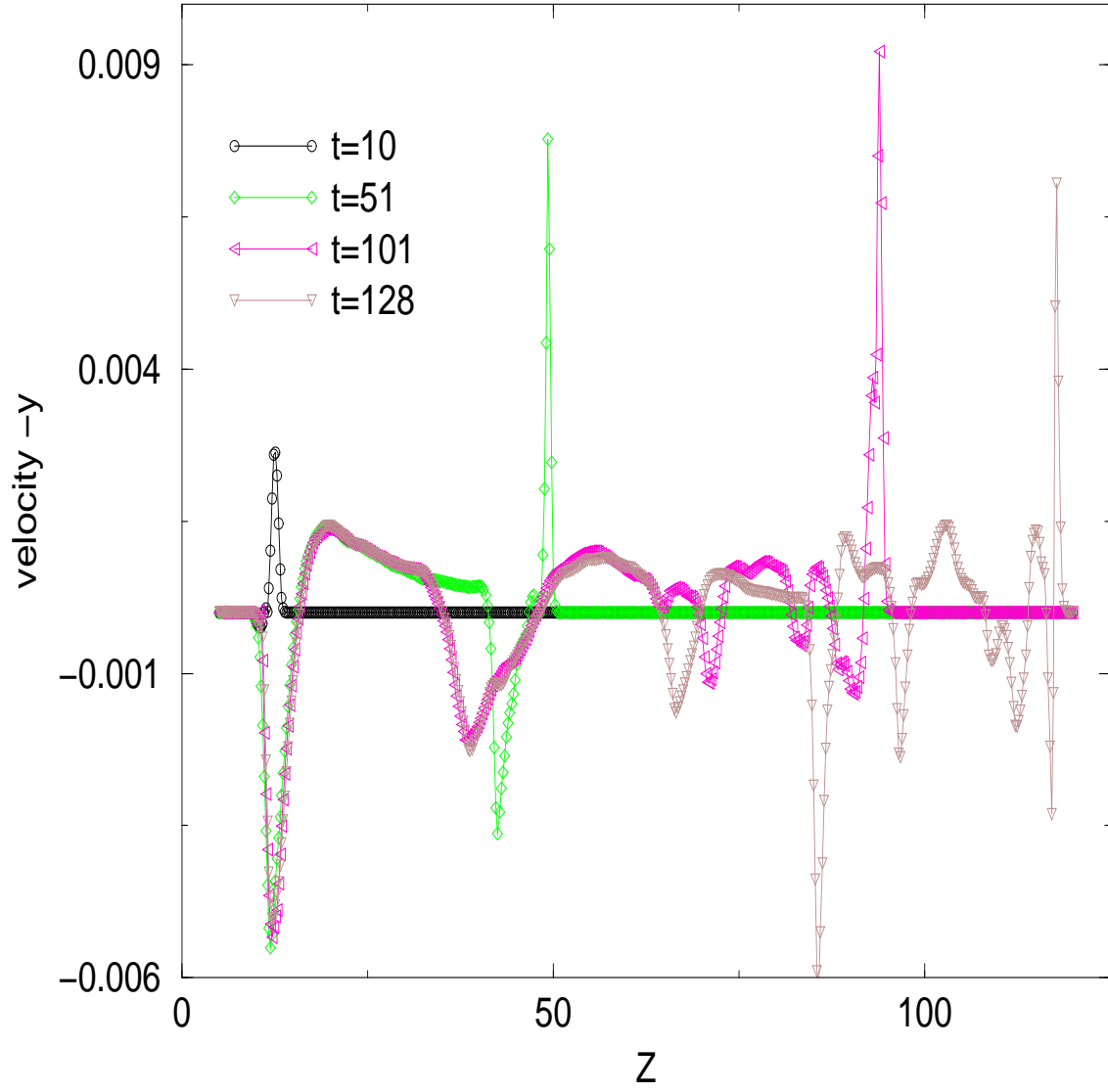


FIG. 8: The  $y$  velocity of relativistic jet at  $y = 5$  at different times as a function of  $Z$ .

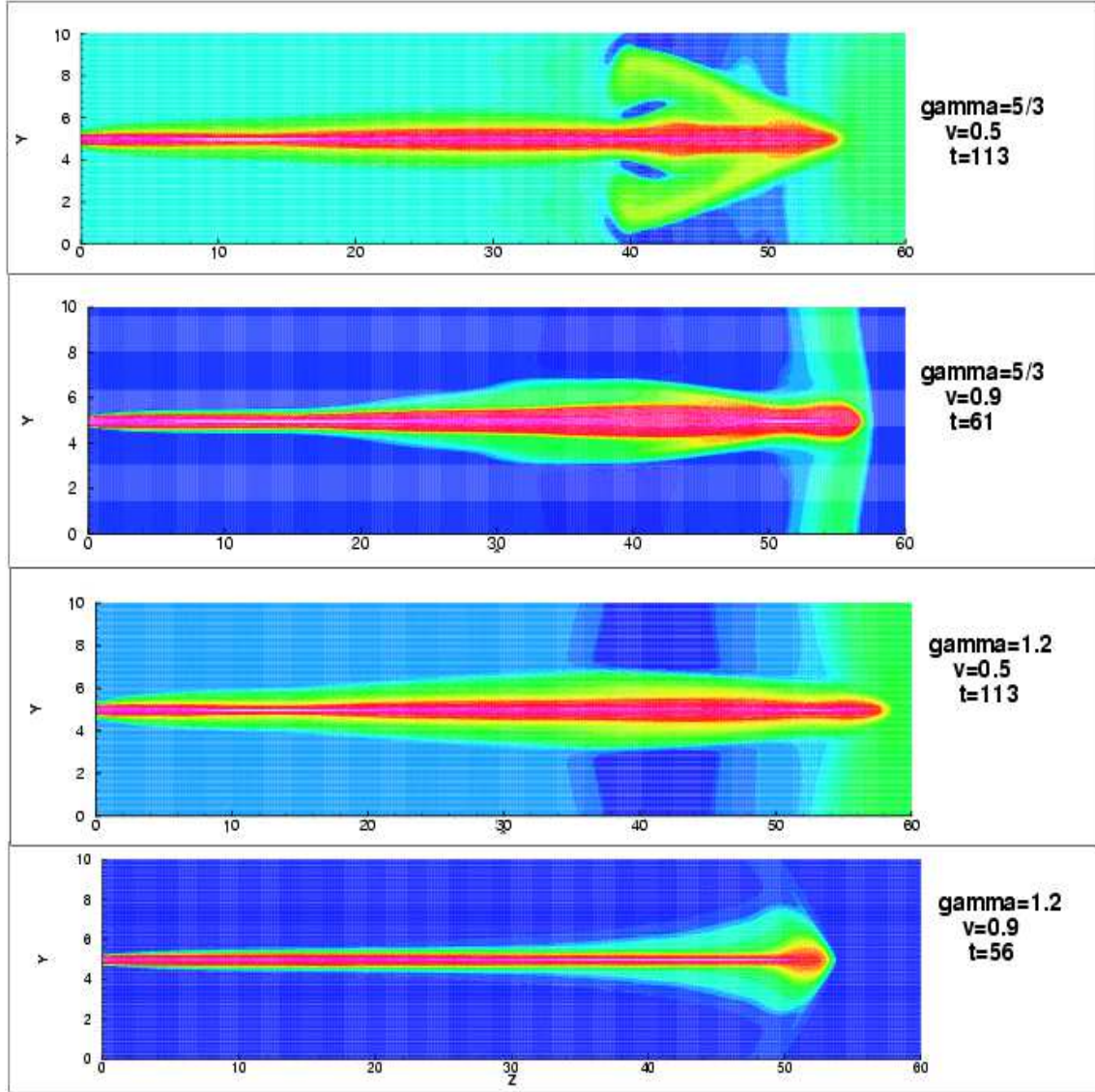


FIG. 9: 2D representation of jet depend of adiabatic index at a fixed time for different jet velocities